

An aeroelastic instability provides a possible basis for the transition from gliding to flapping flight

Oscar M. Curet, Sharon M. Swartz and Kenneth S. Breuer

J. R. Soc. Interface 2013 **10**, 20120940, published online 9 January 2013

References

This article cites 29 articles, 11 of which can be accessed free

<http://rsif.royalsocietypublishing.org/content/10/80/20120940.full.html#ref-list-1>

Subject collections

Articles on similar topics can be found in the following collections

[bioengineering](#) (131 articles)

[biophysics](#) (220 articles)

Email alerting service

Receive free email alerts when new articles cite this article - sign up in the box at the top right-hand corner of the article or click [here](#)



Report

Cite this article: Curet OM, Swartz SM, Breuer KS. 2013 An aeroelastic instability provides a possible basis for the transition from gliding to flapping flight. *J R Soc Interface* 10: 20120940.
<http://dx.doi.org/10.1098/rsif.2012.0940>

Received: 15 November 2012

Accepted: 13 December 2012

Subject Areas:

biomechanics, biophysics, bioengineering

Keywords:

animal flight, flapping flight, gliding, locomotion, leading edge vortex, flow visualization

Author for correspondence:

Oscar M. Curet
e-mail: ocuret@fau.edu

[†]Present address: Department of Ocean and Mechanical Engineering, Florida Atlantic University, Boca Raton, FL, USA.

Electronic supplementary material is available at <http://dx.doi.org/10.1098/rsif.2012.0940> or via <http://rsif.royalsocietypublishing.org>.

An aeroelastic instability provides a possible basis for the transition from gliding to flapping flight

Oscar M. Curet^{1,†}, Sharon M. Swartz^{1,2} and Kenneth S. Breuer^{1,2}

¹School of Engineering, and ²Department of Ecology and Evolutionary Biology, Brown University, Providence, RI, USA

The morphology, kinematics and stiffness properties of lifting surfaces play a key role in the aerodynamic performance of vertebrate flight. These surfaces, as a result of their flexible nature, may move both actively, owing to muscle contraction, and passively, in reaction to fluid forces. However, the nature and implications of this fluid–structure interaction are not well understood. Here, we study passive flight (flight with no active wing actuation) and explore a physical mechanism that leads to the emergence of a natural flapping motion. We model a vertebrate wing with a compliant shoulder and the ability to camber with an idealized physical model consisting of a cantilevered flat plate with a hinged trailing flap. We find that at low wind speed the wing is stationary, but at a critical speed the wing spontaneously flaps. The lift coefficient is significantly enhanced once the wing starts to oscillate, although this increase in lift generation is accompanied by an increase in drag. Flow visualization suggests that a strong leading edge vortex attached to the wing during downstroke is the primary mechanism responsible for the enhanced lift. The flapping instability we observe suggests a possible scenario for an evolutionary transition from gliding to powered flapping flight in animals that possess compliant wings capable of passive camber. Although the flapping state is accompanied by a lower lift-to-drag ratio, the increased lifting capability it confers might have enabled increased body mass, improved foraging performance and/or flight at lower speeds, any of which might have been selectively advantageous.

1. Introduction

The empirical study of interactions of the wings of animals in flight with the surrounding air poses great technical challenges. Tracking the intricate movements of the three-dimensionally complex wings [1] is only the first difficulty. Investigators may perform flow visualization and measure forces from animals performing natural behaviours, distinguish between actuated and not-actuated motion, etc., although such studies are difficult to execute successfully. Many questions in bio-fluid dynamics, however, cannot be addressed most effectively, or at all, with living animals [2]. Physical modelling presents a powerful means to gain fundamental insights into relevant phenomena in such situations [3]. This general approach has been adopted in diverse ways by biological and physical scientists to better understand aerodynamic performance of wing models at low Reynolds number ($Re < 10^5$), including wings at constant speed [4,5], in rotational motion [6], following an impulsive start [7], exhibiting oscillatory motion [8,9] and with compliant structures [10]. Here, we use a physical model to explore the transition from steady gliding to flapping flight. Our model captures two key features present in many animals: (i) the wing structure can deflect with a restoring stiffness provided, at least in part, by elements of the wing structure, such as shoulder muscles and tendons, and (ii) the lifting surface possesses the ability to change camber due to aerodynamic forces. We embody these characteristics in a highly idealized way using a physical model composed of a cantilevered flat plate, which captures compliance, and a hinged trailing flap, which models variable camber

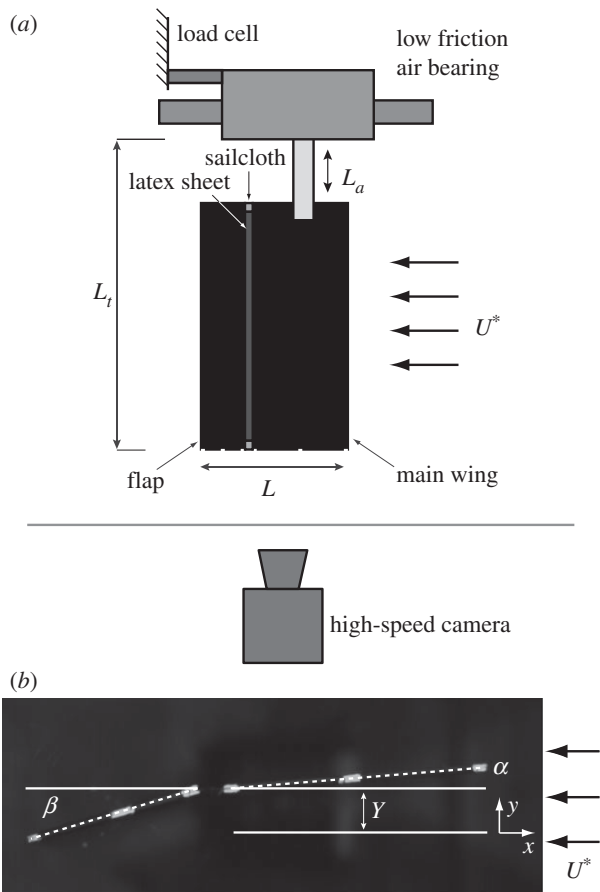


Figure 1. Experimental set-up. (a) Schematic of the experimental set-up. The wing model was mounted on a two-axis air-bearing attached to two uniaxial load cells. A high-speed camera was used to capture kinematics. L_a is the length of the cantilever, L is the chord of the wing, L_t is the length from the edge tip of the wing to the pivot point and $U^* = U/U_{cr}$. (b) Image taken by high-speed camera. Broken white line shows the edge of the wing, as viewed from below (see (a)). α is the angle of attack based on the main wing, β the angle of the flap, and Y the wing deflection.

(figure 1a). With no ambient flow, the model has a natural flapping frequency, f_o which can be controlled by either adjusting the stiffness of the cantilever that serves as the ‘shoulder’ or changing the mass of the wing. In our experiments, the natural frequency was controlled by changing the length of the cantilever. The model is mounted at a fixed angle of attack, α , in a low turbulence wind tunnel, and the lift and drag characteristics are measured over a range of wind speeds, U .

1.1. Physical characteristics of the gliding–flapping transition

At low wind speeds, the physical model remains stationary and is stable to small disturbances. However, above a critical velocity, U_{cr} , the wing starts to oscillate in a sinusoidal manner, heaving in a manner reminiscent of flapping in animal wings (see figure 2a and electronic supplementary material, movie S1). This is an example of the well-known phenomenon of ‘flutter’ instability, which arises from interaction between an elastic structure and fluid flow. This phenomenon has been studied in aircraft wings [11,12], flags [13], suspension bridges [14], filaments in soap films [15] and other systems. However, our study is distinctive in two important respects: (i) the configuration of the physical model abstracts a biological wing characterized by

camber and compliance, and (ii) we characterize the benefits associated with the onset of flutter from a biological perspective, and do not interpret the unsteady phenomenon as a precursor to aeroelastic failure.

The unsteady motion of the wing, as measured by the standard deviation of the flapping amplitude, $\theta = \arcsin(Y/L_t)$, increases with wind speed $U^* = U/U_{cr}$ and is independent of the initial angle of attack (figure 2b). The flap position, β , exhibits a similar behaviour but with larger magnitude oscillation and with a phase angle that leads by approximately 5 per cent of the total flapping cycle. The frequency of oscillation (figure 2c), represented as a Strouhal number, $St = fL/U$, remains constant over a range of velocities: i.e. the flapping frequency increases linearly with flow speed. However, the flapping frequency is lower than the natural frequency of the wing, f_o ($St/St_o \approx 0.8$, where $St_o = f_o L/U$). The reduction in frequency might be associated with additional damping or a lower effective spring constant, both induced by aerodynamic forces.

Similar aeroelastic instabilities have been observed previously, but the effect this kind of flapping motion on aerodynamic force coefficients has yet to be reported. To our surprise, the self-excited motion of the wing model significantly increases the mean lift coefficient (figure 3a), $C_L = F_L / (0.5\rho U^2 A)$, where F_L is lift, ρ the air density, and A the wing area, including the flap. When U^* rises above unity, there is an abrupt jump in the lift coefficient, followed by a slower decrease as the speed increases further. The maximum lift enhancement, quantified as ratio of maximum C_L to the average subcritical C_L , ranges between 15 and 27 per cent. The drag coefficient, C_D , increases more rapidly than C_L (figure 3b), and hence lift-to-drag ratio drops (figure 3c). The amplitude of the unsteady lift force also rises abruptly at the onset of the flapping motion (figure 3d), and exhibits a hysteretic behaviour characteristic of a Hopf bifurcation [16] (figure 3d, inset), consistent with previously reported stabilities of a similar character [15].

1.2. Flow visualization

At subcritical speeds, and at low angles of attack, e.g. $\alpha = 5^\circ$ (figure 4a), smoke visualization reveals that flow separates at the sharp leading edge of the wing. This separation generates small vortices that are shed into the flow. For $U^* > 1$, the flow is more complex (see figure 4b and electronic supplementary material, movie S2). At the beginning of the downstroke, there is a small leading edge vortex (LEV); this is evident in the flow visualization as particles rotating around a common centre and suggests a region of low pressure. The LEV increases in size as the downstroke progresses, but remains attached to the upper surface of the wing until the end of the downstroke, when it is shed into the flow. The flow structure in the wake at mid-downstroke suggests that the flow reattaches to the wing. During the upstroke, the LEV is significantly smaller and the flow is mostly attached to the wing. The two effects of the LEV—the low-pressure region and the recirculation of the flow on the wing surface—are known to enhance lift in delta-wing aircraft [17], and in flapping flight in insects [18,19], bats [20] and gliding swifts [21]. Indeed, it has been suggested that exploitation of LEVs may have evolved as a mechanism to generate high lift over a wide range of Reynolds numbers in animal flight [22]. Although the mechanisms of LEV stability in flapping wings are not well understood, it has been suggested that low

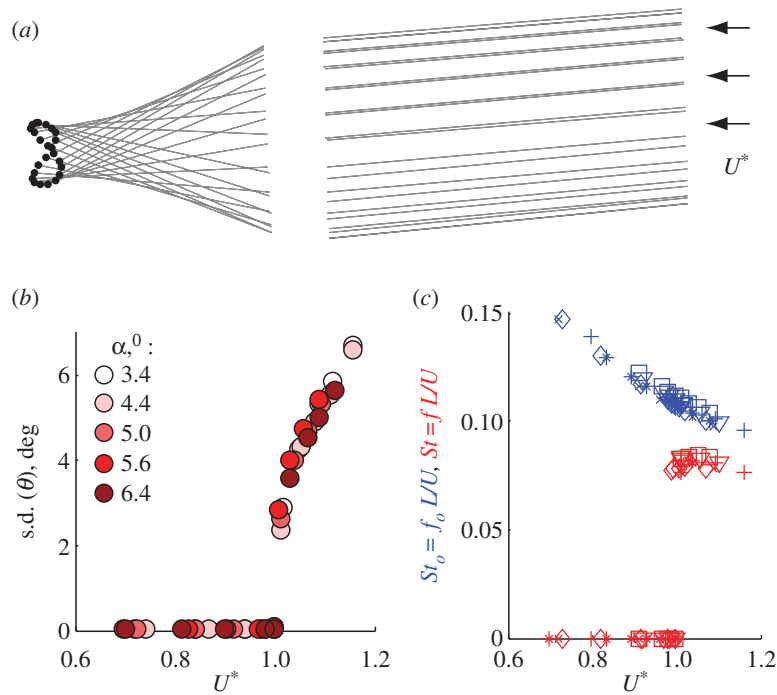


Figure 2. Kinematics of the self-excited flapper. (a) Motion of the flapper at $U^* = 1.01$, $f_o = 4.4$ Hz and $\alpha = 5^\circ$. Solid grey lines show the configuration of the main body and flap at different time instants during one cycle. Black dots show the motion of the trailing edge. (b) Standard deviation of the amplitude of oscillation versus velocity for $f_o = 4.4$ Hz. (c) Strouhal number based on the natural frequency (blue) and the stroke frequency (red) as a function of wind velocity for $\alpha = 5^\circ$. Symbols represent the natural frequency of the model in hertz (in parenthesis the critical velocity in metre per second), squares, $f_o = 3.83$ ($U_{cr} = 4.57$); inverted triangles, $f_o = 3.96$ ($U_{cr} = 4.82$); plus symbols $f_o = 4.26$ ($U_{cr} = 5.13$); cross symbols $f_o = 4.40$ ($U_{cr} = 5.55$); diamonds $f_o = 4.59$ ($U_{cr} = 5.71$); asterisks $f_o = 4.88$ ($U_{cr} = 6.03$).

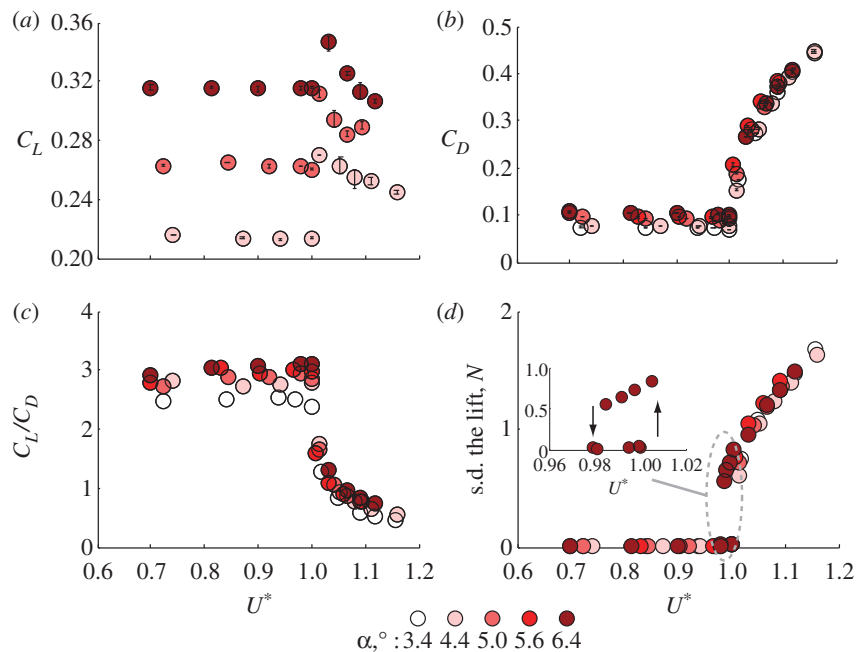


Figure 3. Lift and drag forces on the self-excited flapper. (a) Lift coefficient as a function of wind velocity for $\alpha = 4.4^\circ$, 5.0° and 6.4° . (b) Drag coefficient as a function of wind velocity. (c) Lift-to-drag ratio as function of velocity. (d) Standard deviation of the lift. The inset shows the case for $\alpha = 6.4^\circ$ increasing and decreasing the wind velocity. The error in (a,b) was estimated by the minimum and maximum mean forces.

Rossby number ($Ro = R/c \sim 3$, where R is the wing tip radius and c the wing chord) is a critical parameter for LEV stability [22]. In our case, the Ro ranges from 2.3 to 2.5.

1.3. Implications for biological flight

These results demonstrate that a compliant wing with ability to camber can exhibit a flapping behaviour in steady flow,

without powered actuation. Although the wing model used in this work is an abstraction of biological wings, it captures key features present in animal morphology (camber and compliance) and the observed instability occurs in a Reynolds number regime ($Re = UL/\mu \approx 10^3$, where μ is the kinematic viscosity of air) for animal flight [22]. This suggests that a similar passive motion could arise in wings of gliding animals. Such oscillatory motion could present challenges for

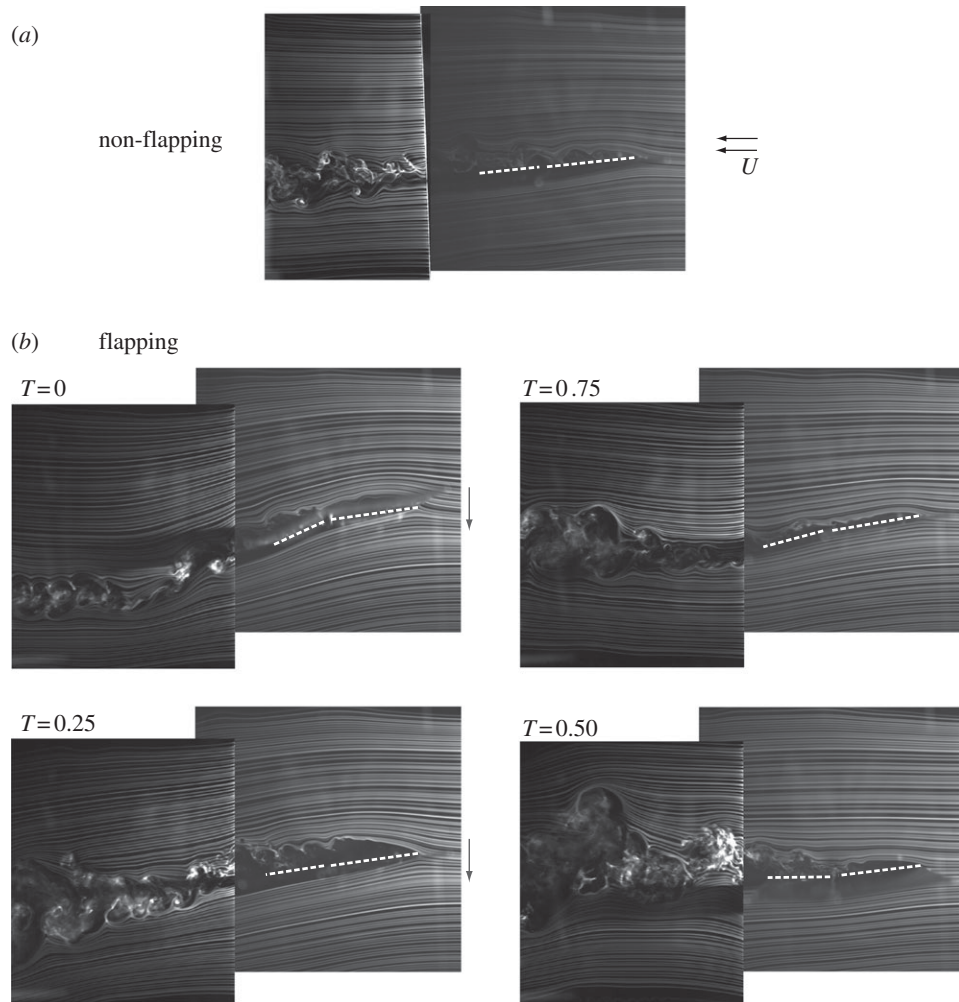


Figure 4. Smoke visualization around the wind model at mid-span. White broken line shows the location of the wing. (a) The wing is in a non-flapping state, $U = 1.0 \text{ m s}^{-1}$. (b) Flow visualization at four times on the flapping cycle, $U = 1.94 \text{ m s}^{-1}$. Starting from the left top panel and counter-clockwise: starting of the downstroke, mid-downstroke, starting upstroke and mid-upstroke. Grey arrows show the direction of the main wing motion. The flow around and behind the wing were recorded separately and stitched together manually.

stability and control during gliding. In a lineage of gliding animals in which such oscillations occur, adaptations of the neuromuscular apparatus that effectively control these motions would be advantageous, and such traits would also be appropriate evolutionary precursors for the ability to control and actuate flapping flight. In addition, our results suggest that small movements of wing membranes—which can be seen to control attitude and trajectory in gliding mammals [23]—could also confer aerodynamic benefits.

This study demonstrates that substantial lift is generated by passive flapping motions, and biological analogues of this flapper model would experience similar increases in aerodynamic force. Furthermore, these passive flapping motions arise from the fluid–wing interaction, and occur close to the resonance of the structure, where compliant wings generate force more effectively than those that are more rigid [24,25]. However, the nondimensional frequency in these experiments, based on stroke amplitude and frequency, $K = fA/U$ where $A = 2L_t \sin(\theta)$, ranges from 0.01 to 0.07, which is considerably lower than those observed for flying animals (from 0.2 to 0.4) [26]. While passive mechanisms might thus be sufficient to initiate flapping, powered actuation may still be required to increase the flapping amplitude and/or frequency, thus raising the nondimensional frequency to a value that might be more energetically beneficial.

We propose that these results offer insight into possible evolutionary trajectories between gliding and flapping flight. Compliant wings capable of passive camber could experience self-excited motion in a manner analogous to that observed in our model. If such self-excited motion is not suppressed, for example, in the absence of muscular contraction, the spontaneous flapping motion could, in turn, produce increased lift due to formation of LEVs. Ultimately, this self-excited motion might have been a precursor to flapping flight of early birds which, based on recent new analysis of fossils, may have used their wings for high-speed gliding [27]. As in our model, animals might experience elevated drag in conjunction with the elevated lift accompanying oscillatory motions. It has often been proposed that improved locomotor economy has driven the evolution of gliding flight [28]. The specialized morphology of gliding animals has thus frequently been interpreted as functioning to maximize lift-to-drag ratio [29]. However, maximizing lift-to-drag ratio may well not have been critical for all gliders, or in the early evolution of flapping flight [30,31]. There are many ecological situations in which this parameter is not necessarily a key target of selection, such as predator escape or capture of elusive but nutritionally rich prey [32]. In settings of these kinds, ‘paying’ for useful lift with additional drag may be an effective compromise to improve

overall fitness. This deviation from 'ideal' steady-state aerodynamics is even more probable in highly transient dynamics such as can be observed in short-range glides [33].

If a lineage of animals that employs gliding locomotion experiences periodic fluttering oscillations that generate elevated aerodynamic forces, could specific patterns of anatomy or neural control be favoured by selection? We hypothesize that specializations of musculoskeletal structure or control might experience positive selection in this locomotor regime. Species with these traits might then be differentially likely to give rise to a lineage of descendants with the capacity for powered flapping, by way of incremental increases in force production capacity and flapping control en route to evolution of a wing. In this way, a simple passive oscillatory physical phenomenon could influence the evolution of muscle-powered flapping flight.

2. Method

The main wing (7.6×28 cm) and flap (5.1×28 cm) were constructed from two pairs of aluminium plates (0.13 cm in thickness) that sandwich two sailcloth straps which allow for easy flexure, and a thin latex sheet which prevents flow from leaking through the gap (0.64 cm) (figure 1a). The natural frequency, f_0 , was controlled by adjusting the length of the supporting cantilever, L_a . The bending stiffness of the main wing-flap connection was much less than that of the cantilever. The flutter speed may be affected by the size of the flap and stiffness of the connection between the main wing and the flap. Characterizing these effects, however, was beyond the scope of this study. To remove the effect of gravity in the model behaviour, the wing was hung from the ceiling of a closed-circuit wind tunnel (test section of $380 \times 60 \times 82$ cm in length, height and width, respectively). The model was mounted on a two-axis platform floating on air bearings. Uniaxial load cells were used to measure drag (22 N, Omega, model LCFA-5) and lift (9 N, Futek, model LSB-200) with a full-scale resolution of 0.7 and 0.3 mN, respectively. For each experimental condition, three trials were recorded at 2000 Hz for 20 seconds each. Before the data acquisition of each experimental set, the load cells were calibrated. The

signals from the load cells were amplified and filtered with a frequency cut-off of 100 Hz using a signal conditioner and amplifier (Vishay Micro-Measurements, model 2310). An additional digital low-pass filter of 20 Hz was performed using MATLAB. The error for the mean lift and drag was estimated by the maximum and minimum average value of the force readings. Drag ranged from 0.02 N during low angle of attack and non-flapping trials to 1.67 N for peak drag forces during flapping. Similarly, lift ranged from 0.05 to 2.80 N. Wing kinematics were recorded at 400 Hz (IDT X-Stream) and synchronized with the force measurements. Three markers each on the main wing and on the flap (figure 1b) were used to track the motion of the flapper. A MATLAB script was used to convert the raw video to binary black and white images, and to identify the centre of the markers for the all the recorded images. The experiments were conducted in a range of free stream wind velocities from 3.5 to 8.5 m s⁻¹.

To visualize flow, smoke was generated using a thin wire (0.22 mm diameter) coated with baby oil and heated resistively. Smoke motion around the model was recorded with a high-speed camera (Photron Fastcam SA3). In two sets of experiments, the smoke wire was placed at mid-span, first in front of the wing and then behind the wing's trailing edge. Because the flow was highly unsteady during flapping, the smoke wire location in front of and behind the wing facilitated observation of flow separation at the leading edge and of the wake behind the wing, respectively. Images from the two series of experiments were stitched together manually. The flow visualization experiments were conducted at lower wind speed to improve the visibility of the smoke. The Reynolds number based on the free stream velocity and chord length was approximately 45 000 and 10 000 for force measurements and flow visualization, respectively.

This work was supported by an AFOSR-MURI on Bioinspired Flight, monitored by Dr Douglas Smith and Dr Willard Larkin. We are grateful to the entire Breuer and Swartz laboratories for their support and camaraderie. K.S.B. and O.M.C. devised the experiment, O.M.C. built the wing model, conducted the experiments and wrote the initial draft of the manuscript. O.M.C., K.S.B. and S.M.S. analysed the data and contributed to the final manuscript.

References

- Lauder GV, Madden PGA. 2008 Advances in comparative physiology from high-speed imaging of animal and fluid motion. *Annu. Rev. Physiol.* **70**, 143–163. (doi:10.1146/annurev.physiol.70.113006.100438)
- Lauder GV. 2011 Swimming hydrodynamics: ten questions and the technical approaches needed to resolve them. *Exp. Fluids* **51**, 3–15. (doi:10.1007/s00348-009-0765-8)
- Koehl MAR. 2003 Physical modelling in biomechanics. *Phil. Trans. R. Soc. Lond. B* **358**, 1589–1596. (doi:10.1098/rstb.2003.1350)
- Spedding GR, Hedenström AH, McArthur J, Rosén M. 2008 The implications of low-speed fixed-wing aerofoil measurements on the analysis and performance of flapping bird wings. *J. Exp. Biol.* **211**, 215–223. (doi:10.1242/jeb.007823)
- Alam M, Zhou Y, Yang H, Guo H, Mi J. 2010 The ultra-low Reynolds number airfoil wake. *Exp. Fluids* **48**, 81–103. (doi:10.1007/s00348-009-0713-7)
- Dickinson M, Lehmann FO, Sane SP. 1999 Wing rotation and the aerodynamic basis of insect flight. *Science* **284**, 1954–1960. (doi:10.1126/science.284.5422.1954)
- Dickinson M, Götz KG. 1993 Unsteady aerodynamic performance of model wings at low Reynolds number. *J. Exp. Biol.* **174**, 45–64.
- Koochesfahani MM. 1989 Vortical patterns in the wake of an oscillating airfoil. *AIAA J.* **27**, 1200–1205. (doi:10.2514/3.10246)
- Anderson JM, Streitlien K, Barrett DS, Triantafyllou MS. 1998 Oscillating foils of high propulsive efficiency. *J. Fluid Mech.* **360**, 41–72. (doi:10.1017/S0022112097008392)
- Heathcote S, Gursul I. 2007 Flexible flapping airfoil propulsion at low Reynolds numbers. *AIAA J.* **45**, 1066–1079. (doi:10.2514/1.25431)
- Theodorsen T. 1935 *General theory of aerodynamic instability and the mechanism of flutter*, no. 496. National Advisory Committee for Aeronautics (NACA).
- Bisplinghoff RL, Ashley H, Halfman RL. 1955 *Aeroelasticity*. Cambridge, MA: Addison-Wesley.
- Argentina M, Mahadevan L. 2005 Fluid-flow-induced flutter of a flag. *Proc. Natl Acad. Sci. USA* **102**, 1829–1834. (doi:10.1073/pnas.0408383102)
- Rocard Y. 1957 *Dynamic instability: automobiles, aircraft, suspension bridges*. New York, NY: Ungar Publication.
- Zhang J, Childress S, Libchaber A, Shelley M. 2000 Flexible filaments in a flowing soap film as a model for one-dimensional flags in a two-dimensional

- wind. *Nature* **408**, 835–839. (doi:10.1038/35048530)
16. Hale JK, Kocak H. 1991 *Dynamics and bifurcations*, 3rd edn. Texts in Applied Mathematics. New York, NY: Springer.
 17. Nelson R, Pelletier A. 2006 The unsteady aerodynamics of slender wings and aircraft undergoing large amplitude maneuvers. *Prog. Aerosp. Sci.* **39**, 185–248. (doi:10.1016/S0376-0421(02)00088-X)
 18. Maxworthy T. 1979 Experiments on the Weis-Fogh mechanism of lift generation by insects in hovering flight. I. Dynamics of the 'fling'. *J. Fluid Mech.* **93**, 47–63. (doi:10.1017/S0022112079001774)
 19. Ellington CP, van den Berg C, Willmott AP, Thomas ALR. 1996 Leading-edge vortices in insect flight. *Nature* **384**, 626–630. (doi:10.1038/384626a0)
 20. Muijres FT, Johansson LC, Bareld R, Wolf M, Spedding GR, Hedenström A. 2008 Leading-edge vortex improves lift in slow flying bats. *Science* **319**, 1250–1253. (doi:10.1126/science.1153019)
 21. Videler JJ, Stamhuis EJ, Povel GDE. 2004 Leading-edge vortex lifts swifts. *Science* **306**, 1960–1962. (doi:10.1126/science.1104682)
 22. Lentink D, Dickinson M. 2009 Rotational accelerations stabilize leading edge vortices on revolving fly wings. *J. Exp. Biol.* **212**, 2705–2719. (doi:10.1242/jeb.022269)
 23. Bishop K. 2006 The relationship between 3-D kinematics and gliding performance in the southern flying squirrel, *Glaucomys volans*. *J. Exp. Biol.* **209**, 689–701. (doi:10.1242/jeb.02062)
 24. Michelin S, Llewellyn Smith SG. 2009 Resonance and propulsion performance of a heaving flexible wing. *Phys. Fluids* **21**, 71902. (doi:10.1063/1.3177356)
 25. Thiria B, Godoy-Diana R. 2010 How wing compliance drives the efficiency of self-propelled flapping flyers. *Phys. Rev. E* **82**, 015303.
 26. Graham KT, Nudds RL, Thomas ALR. 2003 Flying and swimming animals cruise at a Strouhal number tuned for high power efficiency. *Nature* **425**, 707–711. (doi:10.1038/nature02000)
 27. Longrich NR, Vinther J, Meng Q, Li Q, Russell AP. 2012 Primitive wing feather arrangement in *Archaeopteryx lithographica* and *Anchiornis huxleyi*. *Curr. Biol.* **22**, 2262–2267. (doi:10.1016/j.cub.2012.09.052)
 28. Norberg UM. 1985 Evolution of vertebrate flight: an aerodynamic model for the transition from gliding to active flight. *Am. Nat.* **126**, 303–327. (doi:10.1086/284419)
 29. Thorington RW, Santana EM. 2007 How to make a flying squirrel: *Glaucomys* anatomy in phylogenetic perspective. *J. Mammal.* **88**, 882. (doi:10.1644/06-MAMM-S-325R2.1)
 30. Byrnes G, Libby T, Lim NTL, Spence AJ. 2011 Gliding saves time but not energy in Malayan colugos. *J. Exp. Biol.* **214**, 2690–2696. (doi:10.1242/jeb.052993)
 31. Byrnes G, Spence AJ. 2011 Ecological and biomechanical insights into the evolution of gliding in mammals. *Integr. Comp. Biol.* **51**, 991. (doi:10.1093/icb/icc069)
 32. Willis D, Bahlman J, Breuer K, Swartz S. 2011 Energetically optimal short-range gliding trajectories for gliding animals. *AIAA J.* **49**, 2650–2657. (doi:10.2514/1.J051070)
 33. Bahlman JW, Riskin DK, Swartz SM, Breuer KS. 2013 Glide performance and aerodynamics of non-equilibrium glides in Northern flying squirrels (*Glaucomys sabrinus*). *J. R. Soc. Interface* **10**, 20120794. (doi:10.1098/rsif.2012.0794)